Journal of Power Sources 506 (2021) 230110

Contents lists available at ScienceDirect

Journal of Power Sources

journal homepage: www.elsevier.com/locate/jpowsour

Measuring the reversible heat of lithium-ion cells via current pulses for modeling of temperature dynamics

B. Bedürftig [a,*], M. Oldenburger [b,c], T. Hüfner [b], E. Richter [b], R.D. Braatz [d], A. Gruhle [e], R. Findeisen [a]

[a] Laboratory for Systems Theory and Automatic Control, University of Magdeburg, Universitätsplatz 2, 39106 Magdeburg, Germany
[b] Daimler AG, Research & Development, Wilhelm-Runge-Str. 11, 89081 Ulm, Germany
[c] Department of Electron Microscopy of Materials Science, University of Ulm, Helmholtzstraße 16, 89081 Ulm, Germany
[d] Massachusetts Institute of Technology, Cambridge, 02139 MA, USA
[e] Farasis Energy Europe GmbH, Benzstraße 2, 72636 Frickenhausen, Germany

ABSTRACT

This article introduces a novel calorimetric measurement method, namely the 'Double Pulse Method', to measure reversible heat in lithium-ion battery cells. In Li-ion cells, reversible heat has a material-dependent characteristic as it is closely related to both entropy change and the temperature dependence of the open circuit voltage. The proposed method measures reversible heat as a highly resolved function of the cell's state of charge. The determination of reversible heat is based on the evaluation of the temperature difference generated by two current pulses of opposite polarity. Unlike established potentiometric methods, the Double Pulse Method is simple to set up, fast, and cost-effective. The accuracy of the Double Pulse Method is demonstrated for an automotive lithium iron phosphate (LFP) cell, and the entropy changes are compared with measurements of the same cell using the established potentiometric method. Simulation results indicate that the cell temperature is more accurate when determined by the reversible heat measurement obtained by the Double Pulse Method than from the potentiometric method.

1. Introduction

An accurate prediction of the temperature change of the cell during operation is needed when designing optimal battery and thermal management systems based on new Li-ion battery designs [1–3]. Knowledge of the battery temperature and its dynamics at different operating conditions is essential to satisfy safety and aging requirements, and to prevent battery damage in fast charging applications. In the industrial field, the growing number of commercially available cells requires a fast and cost-effective modeling of the temperature dynamics of Li-ion battery cells where established measurement methods are becoming unsuitable due to their long measurement time or complex measurement setup. To overcome these problems, we present a novel calorimetric measurement method, namely, the 'Double Pulse Method' (DPM).

The total heat of a Li-ion cell (Q_{tot}) is the sum of irreversible heat (Q_{irr}) and reversible heat (Q_{rev}) [4], where Q_{irr} describes the losses in the cell and Q_{rev} is associated with a change in entropy (ΔS) (see Section 2). Improvements in battery technology have led to decreases in the irreversible heat Q_{irr}. These improvements include thinner separators with a higher ionic conductivity, new active materials with an optimal particle size, electrolytes with a higher ionic conductivity, and a thinner and more homogeneous solid electrolyte interface [5]. Typically, the reversible heat Q_{rev} for Li-ion cells depends on the electrode materials, the state of charge (SOC), and the temperature. The influence of the reversible heat Q_{rev} on total heat Q_{tot} is not negligible and can account for temperature variations in the battery of up to several degrees Kelvin [6,7]. Therefore, an accurate measurement of Q_{rev} is essential for an adequate prediction of the temperature dynamics of Li-ion cells.

A potentiometric method is commonly used to estimate Q_{rev} by measuring the temperature dependence of the open circuit voltage (OCV) (see Section 2.2) [7–14]. A disadvantage of this method in practice is error induced by the superimposed voltage relaxation of the OCV [4,7,10,12]. Eddahech et al. [12], and Schmidt et al. [4] paused cells for 1 to 2 days to reduce the error due to the superimposed voltage relaxation after the SOC was set. However, even after such a long rest time, the cells had not yet reached the equilibrium potential and the errors were in the range of the entropy effect [4]. Osswald et al. [10] reduced the measurement time per SOC operating point to a few hours using a fitting function to correct for the relaxation. However, the quality of the fit has a considerable influence on the ΔS determination.

Long measurement times and the pausing of the cell at one SOC operating point can lead to further problems. Especially for experimental and laboratory cells, self-discharge can have a non-negligible influence. For commercial cells, a part of the anode has no opposite cathode, for

* Corresponding author.
E-mail address: benjamin1.beduerftig@ovgu.de (B. Bedürftig).

https://doi.org/10.1016/j.jpowsour.2021.230110
Received 16 March 2021; Accepted 26 May 2021
Available online 5 June 2021

manufacturing and security reasons. This area is known as the anode overhang [15,16]. Due to long rest times of several hours or days, the anode overhang can still be lithiated or delithiated depending on the anode potential, which can shift the SOC up to 10% [16]. In order to minimize the error caused by the anode overhang, the total measuring time should always be as short as possible.

Another method to obtain the total heat Q_{tot} is via full or fractional cell cycles and measuring the temperature profile while the cell is placed in a calorimeter [6,12,17,18]. By changing the current amplitude, the reversible heat Q_{rev} and change in entropy ΔS can be determined (see Section 2) [12]. Because of increases in cell size, especially in the automotive sector, most standard calorimeters cannot be used due to their small chamber volume, so expensive custom-made setups need to be used. Additionally, the calorimeters have a high potential for errors from a number of sources. Errors can be caused by the cables which connect the cell, heat distribution inside the calorimeter, and external temperature influences. Furthermore, errors due to cell effects such as hysteresis losses and time-dependent internal resistance also occur [19,20].

Besides the described method to determine the reversible heat Q_{rev}, there is also the possibility to measure the emitted heat flux of the cell to the environment. This measurement requires the heat flux sensor to be both calibrated and specially contacted [21]. Another approach to obtain the reversible heat Q_{rev} is thermal impedance spectroscopy, where the cell is excited with a sinusoidal current and the response is transformed into the frequency domain [4]. This procedure allows a separation of the reversible heat Q_{rev} and irreversible heat Q_{irr} from the total heat Q_{tot}. The disadvantages of this method are the required rather complicated generation of the sinusoidal excitation signals and the complex evaluation of the measurement signals in the frequency domain compared to the other methods.

To measure reversible heat in Li-ion cells, the DPM allows for a simple evaluation of the measured signals, the use of cost-effective equipment, and a rather simple measurement setup. The DPM requires neither an expensive calorimeter nor heat flow sensors, and has no special demands on the DC power supply for the current pulses.

The remainder of this article is structured as follows: Section 2 reviews calorimetric and potentiometric basics. Section 3 then explains the idea of the Double Pulse Method, its measurement setup, and its signal evaluation. Section 4 describes the procedure and the improvements over the potentiometric method. An experimental validation of the methods is in Section 5. Section 6 provides a detailed discussion of the determined values of the entropy change. Section 7 concludes with a summary of the findings. The derivation of the change in entropy by using the temperature dependence of the OCV is provided in Appendix.

2. Fundamentals

To derive and discuss the relationship between thermodynamic and electrical quantities of Li-ion cells, we first review the thermodynamic laws and loss mechanisms within cells, to cover all involved fundamental equations and to provide an insight into the fundamental concepts. We show that both the calorimetric and potentiometric methods can be used to determine the change in entropy of Li-ion cells.

2.1. Calorimetric basics

The total heat generated during operation of a Li-ion cell is the sum of irreversible and reversible heat [4],

$$Q_{tot} = Q_{rev} + Q_{irr}, \tag{1}$$

where Q_{irr} describes the loss mechanisms from converting electrical energy into heat.[1] This irreversible part of the generated heat can be expressed as a rate by

$$P_{loss} = \dot{Q}_{irr} = (V_{cell} - V_{OCV})I, \tag{2}$$

where I is the cell current and the difference between the cell voltage V_{cell} and the open circuit voltage (OCV) V_{OCV} is the overpotential. After a current pulse excitation, there are also equilibrium currents in the cell which cause additional heat to be generated. These losses are included in the capacity part (the imaginary part of the impedance) of the overpotential. The stored energy in the capacity, such as the double layer capacity, transfers to heat after the current excitation, which results in a time shift between the heat generation of the relaxation process and the heat generation of the excitation pulse. Consequently, only a portion of the generated heat is expressed by Eq. (2), not its dynamic behavior. Furthermore, Eq. (2) does not consider the losses from OCV hysteresis which inherently occur when changing the SOC [19]. These losses can be related to the area between the charge and discharge branches of the OCV. In particular at higher temperatures, the losses of the OCV hysteresis are significant in total heat generation. A correct calculation of the dynamic behavior would require accurate modeling of all balancing processes within the cell. To reduce the effort of modeling these processes, we propose the 'Double Pulse Method' (DPM) as presented in Section 3, which overcomes this problem. The DPM is based on the measurement of the cell temperature change caused by the excitation of two current pulses of opposite polarity, where the amplitude of the pulses are identical. Due to the impact of the reversible heat Q_{rev} on the temperature, the measured temperature pulses have different values. These differences can be used to determine the entropy change. In order to measure the main amount of the generated heat and to prevent a complex modeling of the relaxation processes, a pause is set after each excitation in which the relaxation processes occur. As a result, the DPM becomes robust against changes in the relaxation process, and in the dynamics of heat generation. The following text is an explanation of thermodynamic fundamentals.

The reversible heat Q_{rev} is related to the total entropy differential by the second law of thermodynamics:

$$dS = \frac{\delta Q_{rev}}{T}, \tag{3}$$

where T is the absolute temperature. This reversible work is contained in the reaction enthalpy [22]. For electrochemical processes, the generated reversible heat can be expressed as a rate by [22]

$$\dot{Q}_{rev} = \frac{I\,T\,\Delta S}{zF}, \tag{4}$$

where ΔS is the change in entropy, F is the Faraday constant, and z is the number of electrons transferred per ion. Eqs. (1) and (4) form the basis of the DPM. Instructions of how to measure $\dot{Q}_{rev}$ are introduced and explained in Section 3.

2.2. Potentiometric basics

For electrochemical processes, the change in entropy ΔS can be determined using the temperature dependence of the OCV [4,10]:

$$\Delta S = z\,F\frac{\partial V_{OCV}}{\partial T}, \tag{5}$$

where V_{OCV} is the open circuit voltage, F is the Faraday constant, and z is the number of electrons transferred per ion. The change in entropy ΔS and the temperature dependence of the OCV are related to thermodynamic potentials and their characteristic equations. The derivation of Eq. (5) and its relationship to the thermodynamic potentials are presented in Appendix.

Using Eqs. (4) and (5), the generated reversible heat part can be expressed as

$$\dot{Q}_{rev} = I\,T\frac{\partial V_{OCV}}{\partial T}. \tag{6}$$

These relations only apply to the relaxed state of the cell, and the associated potentiometric method is presented in Section 4.

[1] For a more detailed discussion of the different loss mechanisms of Li-ion cells, see Jossen [20].

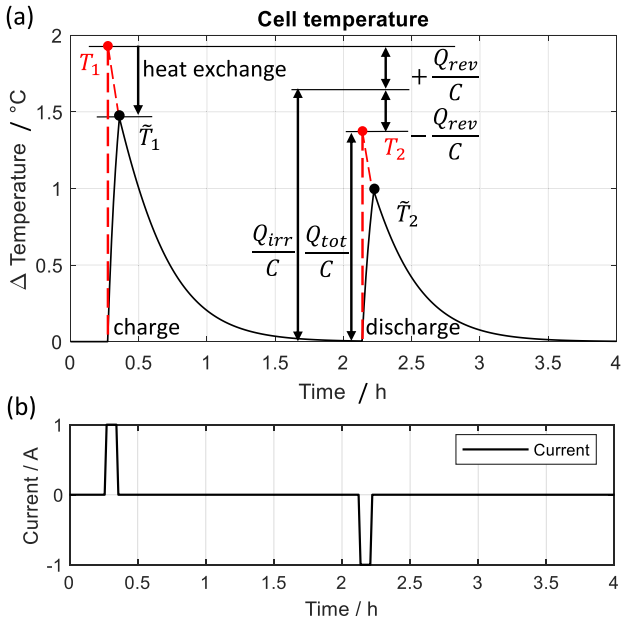

Fig. 1. Cell temperature response of two current pulses of opposite polarity. The theoretical temperature change without heat dissipation to the environment during the current pulse excitation is depicted as dashed lines. The actually measurable temperature is shown as a solid line.

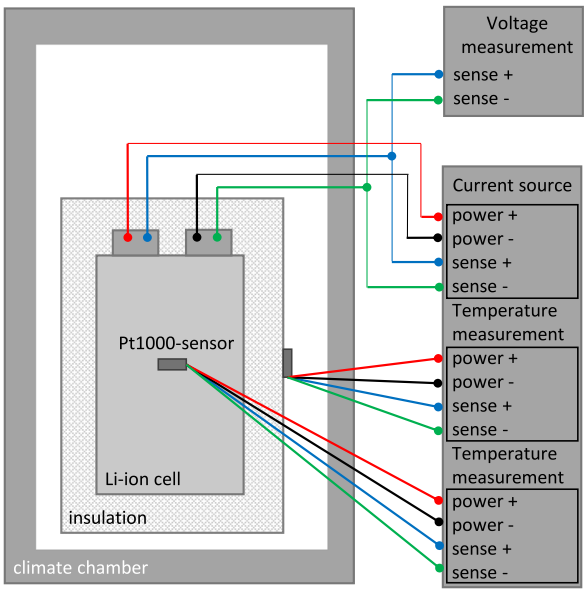

Fig. 2. Connected and insulated cell of the measurement setup of DPM and potentiometric method.

3. The Double Pulse Method (DPM)

To determine the reversible heat Q_{rev} from measurements, we introduce the 'Double Pulse Method' (DPM). The cell is excited by a current pulse charge and discharge of the same amplitude and pulse length (see Fig. 1b). Fig. 1a sketches the temperature response of the cell and shows the relation between the temperatures and the heat generation Q_{tot}, Q_{irr}, and Q_{rev}. Due to the imperfect insulation of the cell, some of the generated heat Q_{tot} is lost during the pulse, and the measured temperatures, $\tilde{T}_1$ and $\tilde{T}_2$, are slightly lower than T_1 and T_2, i.e., the expected values that would occur in the absence of any heat loss.

If the change in entropy ΔS is not equal to 0, the temperature change of the two pulses will differ. From Eq. (4), it is apparent that the reversible heat $\dot{Q}_{\text{rev}}$ depends on the direction of the current. For a positive change in entropy ΔS, the charge currents lead to a positive reversible heat $\dot{Q}_{\text{rev}}$ which additionally heats the cell. For discharge currents, the reversible heat $\dot{Q}_{\text{rev}}$ is negative which cools the cell. The processes reverse at negative change in entropy ΔS. Conversely, the irreversible heat $\dot{Q}_{\text{irr}}$ is always positive (see Eq. (2)). It is therefore possible to determine Q_{rev} from the temperature difference between the two pulses.

Assuming a homogeneous cell temperature and negligible heat losses, the calculation of Q_{rev} can be simplified by using the heat capacity $c_{p,\text{cell}}$ and the mass m of the cell. Regarding the relations shown in Fig. 1, the reversible heat Q_{rev} can be calculated by

$$Q_{\text{rev}} = \frac{Q_{\text{tot}(T_2)} - Q_{\text{tot}(T_1)}}{2} = \frac{1}{2}(T_2 - T_1)\, m\, c_{p,\text{cell}}. \tag{7}$$

The average of $Q_{\text{tot}(T_1)}$ and $Q_{\text{tot}(T_2)}$ can be used to determine irreversible heat:

$$Q_{\text{irr}} = \frac{Q_{\text{tot}(T_2)} + Q_{\text{tot}(T_1)}}{2} = \frac{1}{2}(T_2 + T_1)\, m\, c_{p,\text{cell}}. \tag{8}$$

3.1. DPM measurement setup

When using the DPM, an accurate measurement of the cell temperature change caused by current pulses is important for a correct determination of the reversible heat Q_{rev}. The measurement setup in Fig. 2 is simple and uses low-cost equipment. This measurement setup reduces the influence of typical error sources such as temperature variations of the climate chamber, the contact resistance between the cell taps and the wires, temperature influences due to air convection, and self-heating of the temperature sensors.

The initial step is to connect the cell to a power supply in a 4-wire setup. The cable cross-section of the sense wires should be as thin as possible, the resistance of the power wires should be in the range of the cell resistance, and the contact resistance between cell and wires should be as low as possible. Power wires that are too thin heat the cell, and wires that are too thick drain heat from the cell. In both such cases, the wires would cause a temperature gradient in the cell leading to measurement errors. The parasitic heat generation from the wire itself is not a problem as it is canceled out when applying the DPM.

3.2. Non calorimetry setup correction, DPM

Due to cost, cells are not normally measured using a calorimeter. Thus the total heat Q_{tot} cannot be deduced directly due to the heat exchange between the cell and the environment (see Fig. 1). Instead, Q_{tot} is calculated using Eq. (7) which requires the theoretical temperatures T_1 and T_2 instead of the measured temperature $\tilde{T}_1$ and $\tilde{T}_2$. The theoretical values can be reconstructed using a thermal equivalent circuit model of the cell. Fig. 3 shows this model, where the heat generation rates $\dot{Q}_{\text{irr}}$ and $\dot{Q}_{\text{rev}}$ are modeled as sources, the heat capacity of the cell $c_{p,\text{cell}}$ as capacitor, and the thermal resistances of the insulation ($R_{\text{insulation}}$) and contacted wires (R_{wire}). Compared to the dynamics of the cell, the time constants of the wires are normally much smaller and heat transfer via the insulation has a much larger time constant. Therefore, the dynamics of the wires and insulation typically can be neglected. As such, the thermal capacities of these materials do not have to be modeled in the thermal ECM. As mentioned in Section on DPM Measurement Setup, the cable cross-section (resistance) should be chosen in the range of the cell resistance to avoid high temperature gradients within the cell. The inputs of the ECM are the measured temperature of the environment (climate chamber), $\dot{Q}_{\text{irr}}$, and $\dot{Q}_{\text{rev}}$. Thereby, $\dot{Q}_{\text{irr}}$ and $\dot{Q}_{\text{rev}}$ are functions of the current and the SOC. The constants are the heat capacity of the cell, and the thermal resistance of the wires and insulation. These parameters are fixed and independent of the SOC. Note that the cell temperature is assumed to be homogeneous.

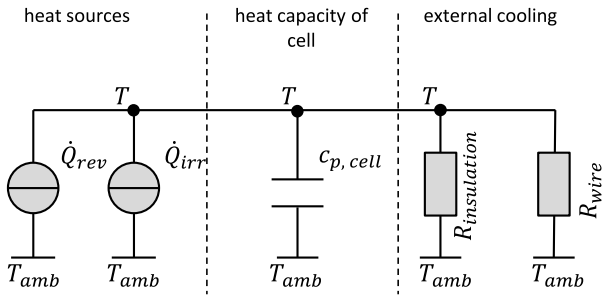

Fig. 3. Thermal equivalent circuit of the measurement setup and the cell, with $\dot{Q}_{\mathrm{rev}}$ and $\dot{Q}_{\mathrm{irr}}$ as sources, the heat capacity of the cell as capacitor $c_{p,\mathrm{cell}}$, and the thermal resistances of the insulation and the contacted wires. T is the temperature of the cell and T_{amb} is the ambient temperature (climate chamber).

The error by the SOC dependence of the internal cell resistance is compensated by the two pulses of opposite polarity, as the amplitude of the pulses are the same.

In the simulation of the thermal equivalent circuit, $\dot{Q}_{\mathrm{irr}}$ and $\dot{Q}_{\mathrm{rev}}$ are varied until the simulated and measured temperature curves of the two excitation pulses match.

4. Measurement procedure of the potentiometric method

In the potentiometric method, the temperature dependence of the OCV is used to determine the entropy change ΔS, as in Eq. (5). After the cell SOC has been set and the equilibrium voltage of the cell has been reached, the cell temperature is changed. Usually, step-wise temperature profiles are used [4,10,12]. However, the cell can take anywhere from several hours to several days to reach equilibrium. If the rest time is insufficient, the temperature dependence of the OCV will be strongly superimposed by relaxation effects which makes the evaluation of the entropy change ΔS impossible [4,10]. Osswald et al. [10] presented a potentiometric method which allows the heat of cells that are not completely relaxed to be measured. To correct influences of relaxation, the voltage drift is estimated by a fit function and subtracted from the measurement signal.

We use a transmission line model (TLM) to determine the voltage drift. The TLM can be derived directly from Fick's laws of diffusion, which enables physics-based modeling of a one-dimensional voltage relaxation to correct the measurement. A possible implementation of the TLM is the 'Cauer model' that corresponds to the telegrapher's equation [19,23]. The resistors of the TLM denote the diffusion velocity, and the capacitors characterize the derivative of the OCV curve at a specific SOC [19]. All elements of the circuit are coupled to each other, which means the voltage of one element is a function of the voltage of all the other elements. An alternative model to correct the voltage drift is the 'Foster model' which has no coupled elements [23]. However, the Foster model cannot reproduce all dynamics. Due to its physical interpretation and easy implementation, we recommend the Cauer model to correct the voltage drift.

In the first step of the correction, the Cauer model is simulated at each SOC point while its parameters are varied until the error between the measured and simulated voltage curves becomes as small as possible. This error is defined as the mean squared error (MSE) and takes into account only measured voltages at the temperature at which the SOC was set. In the next step, the measured voltage curve is subtracted from the simulated voltage. As a result, only the temperature-dependent part of the voltage remains. Finally, Eq. (5) can be used to determine the entropy change.[2] The temperature change within the cell does not occur immediately and an additional complex thermal model would be required to adequately reproduce the cell dynamics.

5. Exemplary experimental validation of the DPM

An LEV21F commercial prismatic cell (from GS Yuasa for automotive applications) with a nominal capacity of 22 Ah was used for the validation. The cell has a graphite anode and a lithium iron phosphate (LFP) cathode. To determine the heat capacity of cells, various methods have been proposed in the literature [6,17,18,24,25]. For commercial Li-ion cells, typical values of the specific heat capacity are in the range of 900–1150 $\frac{\mathrm{J}}{\mathrm{kg\ K}}$ [6,17]. The heat capacity of the LEV21F cell was measured to be 428 $\frac{\mathrm{J}}{\mathrm{K}}$ by immersing an entire cell including the contact tabs into a calorimeter. It is known that the influence of LFP cathodes on the entropy change ΔS is negligible [9,11,13], so the main part of ΔS results from the graphite anode [21]. Thus, the DPM measurements can be compared to results in the literature. Additionally, the established potentiometric method was applied to compare the results. For the potentiometric method, a cell with an LFP cathode is particularly suitable due to its flat OCV characteristic and its smaller amount of the measured voltage relaxation compared to other cathode materials.

5.1. Measurement system and devices

A commercial BaSyTec CTS cell test system was used as current source and for cell monitoring. It is able to set the SOC, to perform temperature measurements, and to generate current pulses for the ΔS determination. The BaSyTec CTS can generate currents from −5 A to 5 A in the voltage range of 0–5 V with a voltage resolution of 0.15 mV and a current resolution of 0.1 μA at a maximum sample rate of 800 Hz.

For temperature measurements, Pt1000 sensors were connected to a separate channel of the BaSyTec CTS by a 4-wire setup. The sensors were fixed in the middle of the cell surface with thermal paste. Hereby a temperature resolution of 0.015 K can be reached with a bias current of 3 mA. Operating the Pt1000 at 3 V was a good compromise between self-heating and voltage resolution. The cell was thermally insulated with 2 cm extruded polystyrene (ESP) and placed in a climate chamber, which has an accuracy of 0.5 K. The insulation should be as hermetic as possible to avoid any heat loss due to air flow to eliminate convective heat transfer [6]. Radiation losses could be minimized by having an emissivity ε as low as possible. Prismatic cells often come with an insulating tape on the surface of the case. We recommend removing this cover to reduce the emissivity. Due to these arrangements, the small temperature variations of the climate chamber are not measurable on the cell surface.

For the potentiometric method, the measurement setup was extended by a Keithley DMM7510 voltmeter which has a resolution of less than 1 μV and can recognize even small OCV changes.

5.2. Measurement setup and measured signals, DPM

For accuracy, select the current amplitude in the range of 0.2–1.0 C with a pulse length of 5% SOC change. If the charge current amplitude is too high, there is a risk of lithium plating occurring at high SOCs. Furthermore, the difference of the cell resistance of 5% SOC change between the charge and discharge direction in the SOC-range of 10%–95% is less than 1%, which keeps errors caused by the current direction-dependent cell impedance low. Additionally, the resolution of the temperature measurement needs to be considered when selecting the current pulse. The setup in Fig. 2 reaches a temperature resolution of 0.015 K with the Pt1000 sensor and the voltage resolution of the BaSyTec CTS. The selected current pulse amplitude and length leads to a typical heating of the cell of about 0.3 K, corresponding to a sufficient resolution of 20 quantization points. In order to minimize effects of Q_{irr} on Q_{tot}, a climate chamber temperature of 25–45 °C should be used.

[2] Although not studied in this work, this parameter estimation procedure should be automatable, which would be useful for industrial applications.

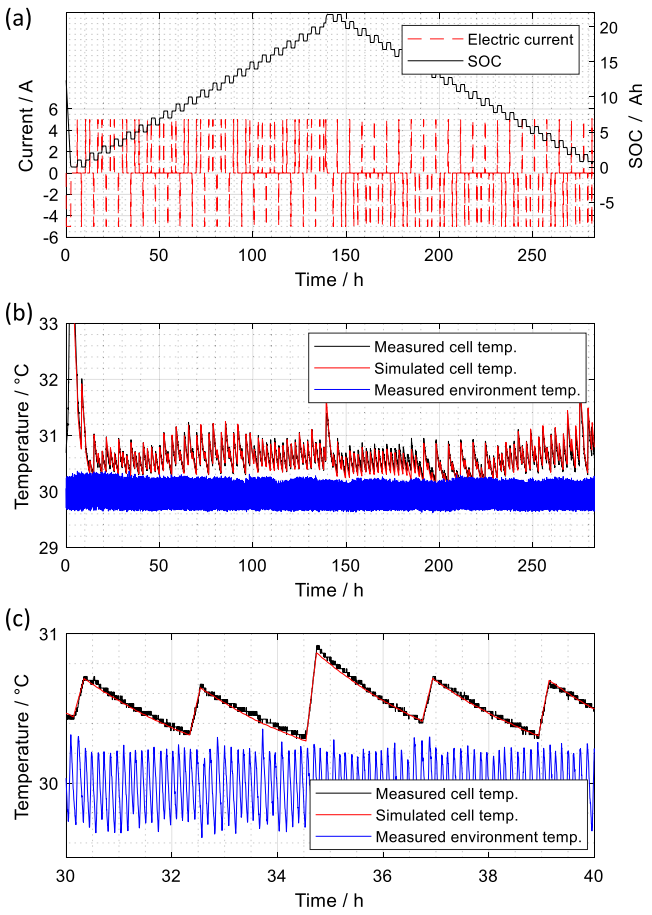

Fig. 4. Measured and simulated signals of the DPM for the LEV21F cell. Excitation current pulses with corresponding (a) SOC, (b) environment and measured and simulated cell temperatures, and (c) a zoomed in plot.

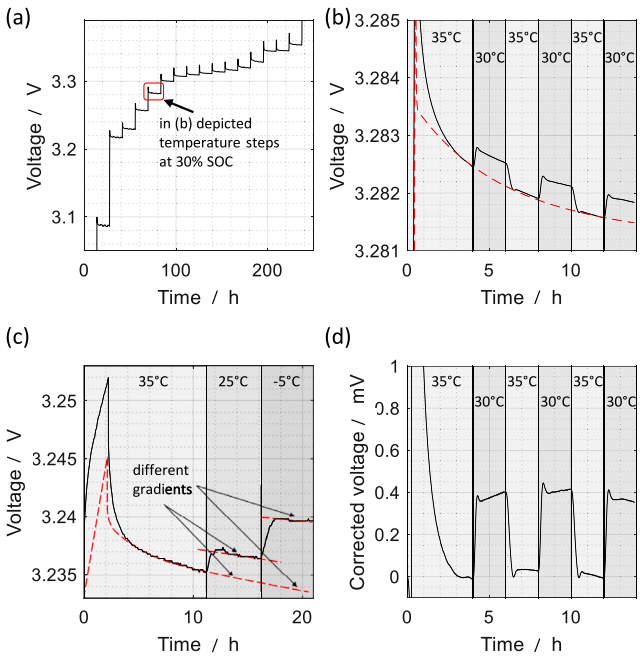

Fig. 5. Measured and simulated signals of the potentiometric method for the LEV21F cell: (a) voltage measurement of the charging branch, (b) measured (solid line) and simulated (red dashed line) voltage at 30% SOC with small temperature variation of the adapted potentiometric method, (c) measured (solid line) and simulated (red dashed line) voltage for a temperature variation that is too high, and (d) drift-corrected cell voltage at 30% SOC with small temperature variation.

At higher temperatures, aging effects can occur such as gas evolution in the cell and side reactions. These effects may lead to measurement errors.

To determine the reversible heat Q_{rev} using the DPM, the LEV21F cell was discharged with 5 A down to 2 V with a cutoff current of C/10. Subsequently, the cell was paused for 4 h to reach a constant cell temperature before starting the pulse excitation. Current pulses with 5 A amplitude and 720 s pulse length were chosen, so the cell was charged or discharged 1 Ah per pulse. For the charge branch, two charge pulses and one discharge pulse excite the cell, which was repeated until the cell voltage reached 3.4 V. Two discharge pulses and one charge pulse were used for the discharging branch. In order to ensure the same start temperature for all pulses, the cell was paused for 2 h after each pulse. This pause is necessary due to the strong temperature dependence of the loss processes occurring in the cell which would influence the measurement of the irreversible heat Q_{irr} and consequently lead to an error in the estimation of the reversible heat Q_{rev}.

For a full charge–discharge cycle, Fig. 4 shows the excitation current, SOC, and temperatures. Using the thermal model in Fig. 3, the temperature decrease after each pulse could be adequately reproduced for the sum of the thermal resistances of the wires and insulation of approximately 20.3 $\frac{\mathrm{K}}{\mathrm{W}}$. The simulated heat transfer to the environment is adjusted until both temperature curves match well (see Fig. 4c), which enables a correction of the environmental influences from the measured temperature $\tilde{T}$ and an accurate determination of $\dot{Q}_{\mathrm{rev}}$ and $\dot{Q}_{\mathrm{irr}}$. As the reversible heat Q_{rev} in Eq. (7) does not depend on R_{wire}, $R_{\mathrm{insulation}}$, or Q_{irr}, Q_{rev} can be determined at each SOC operating point.

Only one physically meaningful combination of all these parameters exists to reproduce the dynamic behavior of all temperature pulses. As a result, errors that occur during the measurement by varying the environment temperature or a change in the contact resistance can be easily detected. In the case of an additional error source, the fixed parameters cannot reproduce all pulses, which can be used as a verification of the quality of the measurement signals and the suitability of the presented model structure. This verification is the advantage of the DPM compared to other measurement methods and allows a clear determination of the reversible heat Q_{rev} for all SOCs.

5.3. Measurement setup and measured signals, potentiometric method

Due to the temperature dependence of the diffusion velocity, only a small range of temperature changes are applicable. In our tests, the SOC was set at 35 °C to ensure rapid relaxation. After the cell was paused for 4 h, the temperature was changed in steps to 30 °C, 35 °C, 30 °C, 35 °C, and 30 °C, with each step taking 2 h.

Fig. 5b is a plot of the measured and simulated voltage relaxation of the presented temperature profile at 30% SOC, and Fig. 5d is the drift-corrected cell voltage at 30% SOC. The high error rate immediately after setting the SOC is due to the fact only one relaxation process was modeled rather than the entire cell.

Due to the small temperature difference of 5 K, a high-resolution voltage measurement was required. A higher temperature step would lead to a larger voltage signal, but high temperature variations result in strong changes in the relaxation time constant as shown in Fig. 5c for a temperature profile of 35 °C, 25 °C, and −5 °C. Corrections of the voltage drift are nearly impossible when there are different relaxation behaviors.

6. Results and discussion

The reversible heat Q_{rev} of the LEV21F cell with an LFP cathode (introduced in Section 5) was determined using the Double Pulse Method.

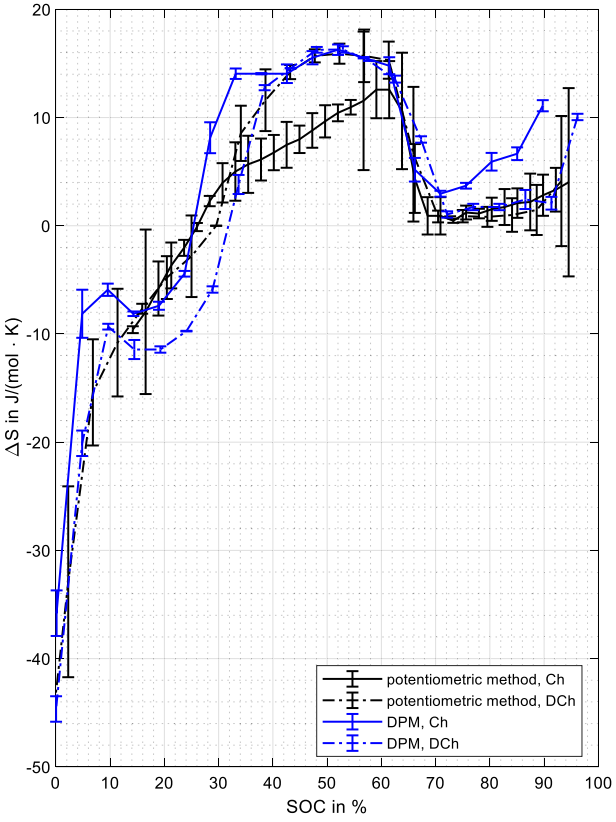

Fig. 6. Comparison of the calculated ΔS curves of the LEV21F cell with the corresponding error bars for DPM and potentiometric method, assuming that the cell is in equilibrium.

The DPM results are validated and verified through comparison with measurements using the potentiometric method and values from the literature. For this purpose, the measured reversible heat Q_{rev} from the DPM and the measured temperature dependence of the OCV from the potentiometric method are used to determine the entropy change ΔS, assuming that the cell is in equilibrium. Furthermore, the calculated Q_{rev} of the DPM and potentiometric method were implemented in the ECM in Fig. 2 in order to simulate and compare the cell temperature to its measured values.

Fig. 6 shows the resulting entropy change ΔS curves of the DPM and potentiometric method as a function of the SOC for both the charge and discharge branch. As outlined in Section 2, the ΔS curves can have positive or negative values. The ΔS curves have the same characteristic profiles reported in the literature [4,7,11,13,17]. In the potentiometric method, for SOCs below 15%, ΔS values of the charge branch could not be obtained due to high voltage drift. These drifts are too high and cannot be corrected by the applied transmission line model.

The 95% confidence intervals for the DPM and potentiometric method in Fig. 6 were calculated by the standard deviation of the measurement and the Student's t-distribution [26]. In order to estimate the standard error, the measurements were taken three times. The standard errors of the DPM are in the range of $\pm 2\ \frac{J}{mol\ K}$. As for the potentiometric method, the temperature profile leads to five values of voltage changes which were used to calculate the standard deviation. In the potentiometric method, the standard errors vary from $\pm 3\ \frac{J}{mol\ K}$ to $\pm 8\ \frac{J}{mol\ K}$.

6.1. Comparison of entropy change

Fig. 6 displays the resulting ΔS curves of the DPM and the potentiometric method. All measured ΔS curves qualitatively reproduce

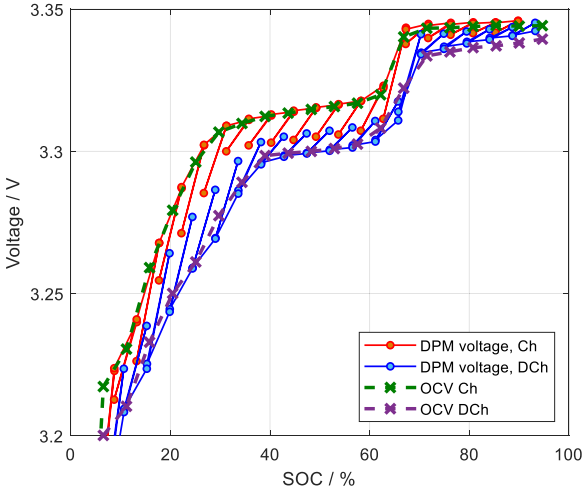

Fig. 7. The recorded voltage at the final position of each SOC point of the DPM and the measured OCV curve at 25 °C for the LEV21F cell.

the characteristic behavior of LFP cells. However, the values of the potentiometric method and the DPM are significantly different at SOC from 0 to 60% for the charge branch and from 15 to 35% for the discharge branch. The difference of the charge branch is especially significant. Contrary to the results of the potentiometric method, the ΔS curves of the DPM do not show differences between the charge and discharge branch of the entropy change for cell SOCs from 30 to 60%. For these reasons, the potentiometric method measurements were repeated. However, the results showed the same differences with the DPM curves. Furthermore, the error bars of the potentiometric method are higher and change considerably (see Fig. 6). In particular, these errors occur during phases where the graphite stages of the cell are changing. Allart et al. [27] obtained similar ΔS curves of the charge and discharge branch for a graphite anode using the potentiometric method. As a result of their post-mortem x-ray diffraction (XRD) analysis, they assume that different graphite stages are the reason of the difference between the charge and discharge branch of the entropy change at cell SOCs from 30 to 60% [27]. Contrary to the results of the potentiometric method, the ΔS curves of the DPM do not show differences between the charge and discharge direction for cell SOCs from 30 to 60%.

The differences in the DPM results seem to be an SOC shift. However, an error of the current measurement cannot be the reason for this shift of about 5%. The BaSyTec CTS power supply for the SOC setting has a current accuracy of 1 mA, leading to a charge error of only 0.02%. Errors in the SOC setting at the beginning of the measurement can be neglected because the charge is measured during the entire experiment and the SOC is not adjusted. Additionally, the recorded voltage at the final position of each SOC point of the DPM was compared to the measured OCV curve of the LEV21F cell (see Fig. 7). The comparison shows that both OCVs match well. However, the effect of anode overhang on the ΔS cannot be ruled out by the OCVs shown in Fig. 7. Another aspect could be a violation of the DPM's assumption that the charge and discharge pulses lead to the same irreversible heat Q_{irr} (see Section 3). As already mentioned in Section 5.2, the variation of the cell resistance is less than 1% within one SOC step of 5%. However, the irreversible heat Q_{irr} can be affected by the losses of the OCV hysteresis [19,28]. We assume for the DPM that losses of the OCV hysteresis have exactly the same amount for the charge and discharge direction. A violation of this assumption could lead to this shift in the ΔS curves. By thermal impedance spectroscopy, Schmidt et al. [4] also observed a difference between the charge and discharge direction of the ΔS curves. Note that the method of thermal impedance spectroscopy also has micro-cycles for each sinusoidal excitation. We assume that the different graphite stages in the anode for the charge and discharge

branch are the reason for the ΔS difference. They also cause the OCV hysteresis shown in Fig. 7 and the hysteresis of the cell thickness [29]. However, the reason and quantification of the ΔS difference is not yet fully understood.

6.2. Simulation of cell temperature

In practice, it is not crucial for an adequate prediction of the cell temperature whether the ΔS curves have a hysteresis or whether the losses of the OCV are different for the charge and discharge direction. What is important is a valid selection of the several parts of the battery model and that there are no conflicts between the assumptions. The DPM results allow a convenient implementation of the reversible heat Q_{rev} in a battery model, since the losses of the OCV hysteresis (area between the OCV curves) can be taken into account by dividing them into equal amounts for the charge and discharge direction. In order to investigate the impact of the differences between the calculated Q_{rev} curves on the predictive ability of the cell temperature, a simulation was carried out in which only the Q_{rev} curves were varied and all other parameters were fixed. Note that this simulation is only performed for one profile, further investigations and a more realistic profile are required to determine the accuracy. The applied battery model is based on the ECM of Forgez et al. [7] and the thermal model in Fig. 2. The model inputs are the measurement signals in Fig. 4. Due to their low excitation currents and small temperature changes, a considerable simplification of the cell model can be achieved [30,31]. Additionally, all current pulses have the same amplitude and pulse length. As a result of these assumptions, the electrical part of the cell model consists of only one internal resistor, which represents all irreversible losses including the losses of hysteresis. By evaluating Eq. (8), the value of the internal resistance can be determined. For SOCs from 20 to 50% the resistance is about 13 mΩ. Thermal parameters of the cell model are the heat capacity of 428 $\frac{J}{K}$ and the simplified heat transfer resistance to the environment of 20.3 $\frac{K}{W}$.[3] The simulation results are displayed in Fig. 8. A comparison of the temperatures shows that using the Q_{rev} curves of the DPM and the simplified cell model can reproduce the measurements. In contrast, the calculated reversible heat Q_{rev} curves of the potentiometric method lead to relative errors up to 40%. Forges et al. [7] also reported a high impact of Q_{rev} on their temperature simulation using a thermal ECM. A temperature offset of the simulation cannot be the reason for the different temperature curves, because the start temperature was the same for both simulations. Furthermore, the error becomes smaller after the discharge pulses at 50 h, 56.5 h, and 64 h and increases after the subsequent charge pulses, corresponding to the differences of the entropy change ΔS curves of Fig. 6.

The potentiometric method seems more suitable for simulating and predicting the temperature dependence of the voltage, which could be important for SOC prediction methods via OCV. For most applications, however, this error is negligible compared to error sources such as self-discharge and anode overhang.

7. Summary

A novel 'Double Pulse Method' (DPM) method is proposed for measuring the reversible heat generation in lithium-ion battery cells by exciting the cell with current pulses. By subtracting the resulting temperature increases of two current pulses of opposite polarity, the reversible heat Q_{rev} is calculated. The advantages of the DPM are simple signal evaluation, cost-effective equipment, and simple setup. Neither heat flow sensors nor expensive calorimeters are required and there is no special demand on the DC power supply for the current pulses. A typical measurement run takes about 11 days. The error of the calculated entropy change ΔS is in the range of ± 2 $\frac{J}{mol\ K}$. The measurement setup can be easily extended to any cell format and cell size.

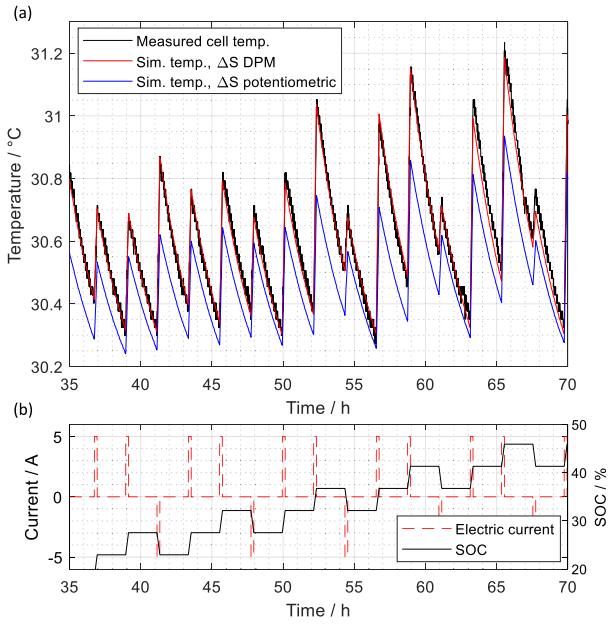

Fig. 8. Simulation results and measurements for the LEV21F cell at 30 °C, whereby only the Q_{rev} curves were varied in the simulation. The other model parameters are fixed. The model inputs are the current and the environment temperature in Fig. 4. For reasons of clarity, the signals were shown in the SOC range from 20 to 50%, where the difference of the entropy change ΔS curves is maximum.

The calculated entropy change ΔS curves from the measured reversible heat Q_{rev} of the DPM were validated by our own potentiometric measurements and values in the literature. All entropy change ΔS curves qualitatively reproduced the characteristic behavior of LFP cells. However, the ΔS curves of the DPM indicate that there is a difference between the charge and discharge direction that could not be observed when using the potentiometric method. The reasons for this observation could not be determined, and repeating the measurements did not eliminate the differences. Further research is needed to clarify if there is indeed a hysteresis of the ΔS function.

Finally, the reversible heat Q_{rev} values of the DPM and potentiometric method were applied to simulate the cell temperature. A comparison of the simulated temperatures shows that the reversible heat Q_{rev} of the DPM can adequately reproduce the measured temperature. In contrast, the potentiometric calculated Q_{rev} curves lead to errors of up to 40% of the measured temperature. Based on these results, we recommend the DPM for measuring the reversible heat in Li-ion cells. Its easy measurement setup and signal evaluation as well as the simple implementation of the measured reversible heat Q_{rev} curves give the battery model community the opportunity to test the DPM and possibly improve their thermal models.

Declaration of competing interest

The authors declare that they have no known competing financial interests or personal relationships that could have appeared to influence the work reported in this paper.

Appendix

To collect important thermal dynamic equations, modeling the temperature dynamics of Li-ion cells, and to give a deeper insight into the potentiometric method and its fundamentals, the derivation of ΔS using the temperature dependence of the OCV is presented here. The entropy

[3] The cell was thermally insulated with 2 cm extruded polystyrene (ESP).

change ΔS and the temperature dependence of the OCV are related to thermodynamic potentials and their characteristic equations. The total differential of Gibbs energy is defined as

$$dG = -S\,dT + V\,dp + \sum_i \mu_i\,dN_i \tag{9}$$

and the total differential of the enthalpy is given by

$$dH = T\,dS + V\,dp + \sum_i \mu_i\,dN_i, \tag{10}$$

where V is the volume, p is the pressure, μ is the chemical potential, and N is the particle number. Combining Eqs. (9) and (10), the differential of Gibbs energy can be described by the total differentials of enthalpy, entropy, and temperature:

$$dG = dH - T\,dS - S\,dT. \tag{11}$$

The integral of Eq. (11) from the initial state (is) to the final state (fs) of the reaction, assuming that the start and end temperatures of the reaction are the same, can be expressed as

$$\begin{aligned}\Delta G = \int_{is}^{fs} dG &= \int_{is}^{fs} dH - \int_{is}^{fs} T\,dS - \int_{is}^{fs} S\,dT \\ &= \Delta H - T\,\Delta S.\end{aligned} \tag{12}$$

After an equilibrium is reached, changing the temperature of the system, Eq. (12) can be rewritten as

$$\frac{\partial \Delta G}{\partial T} = \frac{\partial}{\partial T}(\Delta H - T\,\Delta S) = -\Delta S. \tag{13}$$

This equation describes a direct relation between ΔS and the change in Gibbs energy as a function of temperature.

Integrating Eq. (9), assuming that pressure and temperature are the same in the initial state (is) and final state (fs), Eq. (9) can be expressed as

$$\begin{aligned}\Delta G = \int_{is}^{fs} dG &= \int_{is}^{fs} \sum_i \mu_i\,dN_i \\ &= \int_0^1 \sum_i \mu_i\,\nu_i\,d\lambda = \sum_i \mu_i\,\nu_i,\end{aligned} \tag{14}$$

with stoichiometry factor ν and the reaction number λ from 0 to 1.

So far, the change in Gibbs energy G has been described only by the chemical potential μ without including 'external' fields such as the electric field or the gravity field. For Li-ion cells, the electrical work W and the electrochemical potential must be taken into account. If the OCV is established between the two cell electrodes, Faraday's law is expressed as

$$W = z\,F\,V_{\mathrm{OCV}}. \tag{15}$$

Adding this electric work to both sides of Eq. (14), the sum of chemical energy and electrical energy in the electrochemical equilibrium is zero:

$$\Delta G + z\,F\,V_{\mathrm{OCV}} = \sum_i \mu_i\,\nu_i + z\,F\,V_{\mathrm{OCV}} = 0. \tag{16}$$

For reversible electrochemical processes, the change in Gibbs energy can be expressed as

$$\Delta G = -z\,F\,V_{\mathrm{OCV}}. \tag{17}$$

This relation only applies to the relaxed state of the cell. Gibbs energy is thus the maximum extractable energy of a system. By substituting Eq. (17) into Eq. (13), the entropy change ΔS can be determined using the temperature dependence of the OCV:

$$\Delta S = z\,F\,\frac{\partial V_{\mathrm{OCV}}}{\partial T}. \tag{18}$$

References

[1] J. Kim, J. Oh, H. Lee, Review on battery thermal management system for electric vehicles, Appl. Therm. Eng. 149 (2019) 192–212.

[2] U. Krewer, F. Röder, E. Harinath, R. Braatz, B. Bedürftig, R. Findeisen, Review–dynamic models of Li-ion batteries for diagnosis and operation: A review and perspective, J. Electrochem. Soc. 165 (16) (2018) A3656–A3673.

[3] R. Klein, N.A. Chaturvedi, J. Christensen, J. Ahmed, R. Findeisen, A. Kojic, Electrochemical model based observer design for a lithium-ion battery, IEEE Trans. Control Syst. Technol. 21 (2) (2013) 289–301.

[4] J.P. Schmidt, A. Weber, E. Ivers-Tiffée, A novel and precise measuring method for the entropy of lithium-ion cells: ΔS via electrothermal impedance spectroscopy, Electrochim. Acta 137 (2014) 311–319.

[5] K. Zaghib, A. Mauger, H. Groult, J.B. Goodenough, C.M. Julien, Advanced electrodes for high power Li-ion batteries, Materials 6 (3) (2013) 1028–1049.

[6] J.-S. Hong, Electrochemical-calorimetric studies of lithium-ion cells, J. Electrochem. Soc. 145 (5) (1998) 1489–1501.

[7] C. Forgez, D.V. Do, G. Friedrich, M. Morcrette, C. Delacourt, Thermal modeling of a cylindrical $LiFePO_4$/graphite lithium-ion battery, J. Power Sources 195 (9) (2010) 2961–2968.

[8] Y. Reynier, R. Yazami, B. Fultz, The entropy and enthalpy of lithium intercalation into graphite, J. Power Sources 119–121 (2003) 850–855.

[9] V.V. Viswanathan, D. Choi, D. Wang, W. Xu, S. Towne, R.E. Williford, J.-G. Zhang, J. Liu, Z. Yang, Effect of entropy change of lithium intercalation in cathodes and anodes on Li-ion battery thermal management, J. Power Sources 195 (11) (2010) 3720–3729.

[10] P.J. Osswald, M. del Rosario, J. Garche, A. Jossen, H.E. Hoster, Fast and accurate measurement of entropy profiles of commercial lithium-ion cells, Electrochim. Acta 177 (2015) 270–276.

[11] A. Nazari, S. Farhad, Heat generation in lithium-ion batteries with different nominal capacities and chemistries, Appl. Therm. Eng. 125 (2017) 1501–1517.

[12] A. Eddahech, O. Briat, J.-M. Vinassa, Thermal characterization of a high-power lithium-ion battery: Potentiometric and calorimetric measurement of entropy changes, Energy 61 (2013) 432–439.

[13] K. Jalkanen, T. Aho, K. Vuorilehto, Entropy change effects on the thermal behavior of a $LiFePO_4$/graphite lithium-ion cell at different states of charge, J. Power Sources 243 (2013) 354–360.

[14] K. Maher, R. Yazami, Effect of overcharge on entropy and enthalpy of lithium-ion batteries, Electrochim. Acta 101 (2013) 71–78.

[15] M. Lewerenz, J. Münnix, J. Schmalstieg, S. Käbitz, M. Knips, D.U. Sauer, Systematic aging of commercial $LiFePO_4$ | graphite cylindrical cells including a theory explaining rise of capacity during aging, J. Power Sources 345 (2017) 254–263.

[16] T. Hüfner, M. Oldenburger, B. Bedürftig, A. Gruhle, Lithium flow between active area and overhang of graphite anodes as a function of temperature and overhang geometry, J. Energy Storage 24 (2019) 100790.

[17] L. Sheng, L. Su, H. Zhang, Y. Fang, H. Xu, W. Ye, An improved calorimetric method for characterizations of the specific heat and the heat generation rate in a prismatic lithium ion battery cell, Energy Convers. Manage. 180 (2019) 724–732.

[18] K. Onda, T. Ohshima, M. Nakayama, K. Fukuda, T. Araki, Thermal behavior of small lithium-ion battery during rapid charge and discharge cycles, J. Power Sources 158 (1) (2006) 535–542.

[19] M. Oldenburger, B. Bedürftig, A. Gruhle, F. Grimsmann, E. Richter, R. Findeisen, A. Hintennach, Investigation of the low frequency Warburg impedance of Li-ion cells by frequency domain measurements, J. Energy Storage 21 (2019) 272–280.

[20] A. Jossen, Fundamentals of battery dynamics, J. Power Sources 154 (3) (2006) 530–538.

[21] K.A. Murashko, A.V. Mityakov, V.Y. Mityakov, S.Z. Sapozhnikov, J. Jokiniemi, J. Pyrhönen, Determination of the entropy change profile of a cylindrical lithium-ion battery by heat flux measurements, J. Power Sources 330 (2016) 61–69.

[22] D. Bernardi, E. Pawlikowski, J. Newman, A general energy balance for battery systems, J. Electrochem. Soc. 132 (1) (1985) 5–12.

[23] E. Kuhn, C. Forgez, P. Lagonotte, G. Friedrich, Modelling Ni-mH battery using Cauer and Foster structures, J. Power Sources 158 (2) (2006) 1490–1497.

[24] H. Maleki, S. Al-Hallaj, J. R. Selman, R. Dinwiddie, H. Wang, Thermal properties of lithium-ion battery and components, J. Electrochem. Soc. 146 (3) (1999) 947–954.

[25] S.J. Bazinski, X. Wang, Experimental study on the influence of temperature and state-of-charge on the thermophysical properties of an LFP pouch cell, J. Power Sources 293 (2015) 283–291.

[26] A. Nicholls, Confidence limits, error bars and method comparison in molecular modeling. Part 1: The calculation of confidence intervals, J. Comput. Aided Mol. Des. 28 (2014) 887–918.

[27] D. Allart, M. Montaru, H. Gualous, Model of lithium intercalation into graphite by potentiometric analysis with equilibrium and entropy change curves of graphite electrode, J. Electrochem. Soc. 165 (1) (2018) A380–A387.

[28] M. Oldenburger, B. Bedürftig, E. Richter, R. Findeisen, A. Hintennach, A. Gruhle, Analysis of low frequency impedance hysteresis of Li-ion cells by time- and frequency domain measurements and its relation to the OCV hysteresis, J. Energy Storage (ISSN: 2352-152X) 26 (2019) 101000.

[29] F. Grimsmann, F. Brauchle, T. Gerbert, A. Gruhle, M. Knipper, J. Parisi, Hysteresis and current dependence of the thickness change of lithium-ion cells with graphite anode, J. Energy Storage 12 (2017) 132–137.

[30] M. Oldenburger, B. Bedürftig, A. Gruhle, E. Richter, A new approach to measure the non-linear Butler–Volmer behavior of electrochemical systems in the time domain, J. Energy Storage 14 (2017) 16–21.

[31] S. Buller, M. Thele, E. Karden, R.W. De Doncker, Impedance-based non-linear dynamic battery modeling for automotive applications, J. Power Sources 113 (2) (2003) 422–430.